International Journal of Nanomedicine

Dovepress
Taylor & Francis Group

Open Access Full Text Article

ORIGINAL RESEARCH

# Amelioration of Inflammation and Metabolic Blockage in GALC Deficient Mice After Enzyme Replacement Therapy via Extracellular Vesicles

Diego Zelada[1,*], Natalia Saldivia[1,*], Shayla Samano[1], Diann George[1], Kenvi Chaudhari[1], Duc Nguyen[1], Daniel Simchuk[2], Richard B Van Breemen[2], Maria Irene Givogri[1]

[1]Department of Anatomy and Cell Biology, College of Medicine. University of Illinois Chicago, Chicago, IL, 60612, USA; [2]Linus Pauling Institute, Oregon State University, Corvallis, OR, 97331, USA

*These authors contributed equally to this work

Correspondence: Maria Irene Givogri, Department of Anatomy and Cell Biology, College of Medicine, University of Illinois at Chicago, 808 S, Wood St, M/C 512, Chicago, IL, 60612, USA, Email mgivogri@uic.edu

**Introduction:** Krabbe disease (KD) is a fatal lysosomal storage disorder caused by a deficiency in the enzyme galactosylceramidase (GALC), leading to toxic accumulation of psychosine. This results in widespread demyelination, inflammation, and neuronal damage. Early intervention is critical to mitigate disease progression and limit neurological injury.

**Methods:** To assess the therapeutic potential of early enzyme replacement therapy (ERT), HeLa cells were genetically engineered to overexpress GALC, and extracellular vesicles (EVs) containing GALC were isolated. A single intrathecal injection of these GALC-loaded EVs was administered to neonatal GALC-deficient twitcher mice, a well-established model of KD.

**Results:** Although the treatment did not prolong overall survival, it significantly reduced neuroinflammation. Treated mice exhibited decreased astrogliosis and microgliosis, along with a notable reduction in cortical psychosine levels. Molecular analysis of neuroinflammatory markers showed increased expression of IL-10 and TREM2 in microglial cells following treatment.

**Discussion:** This study demonstrates that early intervention with GALC-loaded EVs can temporarily alleviate central neuropathology in KD by reducing inflammation and psychosine burden. While not curative, this approach shows potential as an adjunctive strategy to delay disease progression and improve the neuroinflammatory environment prior to hematopoietic stem cell transplantation.

**Keywords:** Krabbe disease, intrathecal injection, galactosylceramidase delivery, psychosine, microglia

## Introduction

Krabbe disease (KD) is caused by a deficiency in the lysosomal enzyme galactosylceramidase (GALC), resulting in the toxic accumulation of galactosylceramide, and galactosylsphingosine (also known as psychosine), primarily in lysosomes and cellular membranes.[1,2] Psychosine is the main driver of neuropathology in KD, leading to widespread demyelination, gliosis, inflammation, and neuronal degeneration.[1,3] Clinical signs typically emerge several weeks or months after birth. However, the underlying pathology begins during the later stages of embryonic development, with psychosine accumulation already significantly elevated in the neonatal brain.[2,4] This underscores the need to study early interventions to reduce psychosine, as early toxicity negatively impacts on the efficacy of subsequent treatments.[5–7] Evidence from hematopoietic stem cell transplantation (HSCT) and gene therapy in the twitcher mouse (Twi), a model of infantile KD, demonstrate that earlier treatment is more effective.[6–8] In this regard, ongoing clinical trials for KD using AAV gene therapy have been discontinued, raising the need of alternative strategies to address the fast progression of the disease in neonates.

Lysosomal enzymes have the common property of following the secretory vesicular pathway and the possibility of being secreted to the extracellular milieu and cross-correct neighbor cells by either by direct cell-to-cell transfer or via

Received: 7 March 2025
Accepted: 8 July 2025
Published: 17 July 2025

**Graphical Abstract**

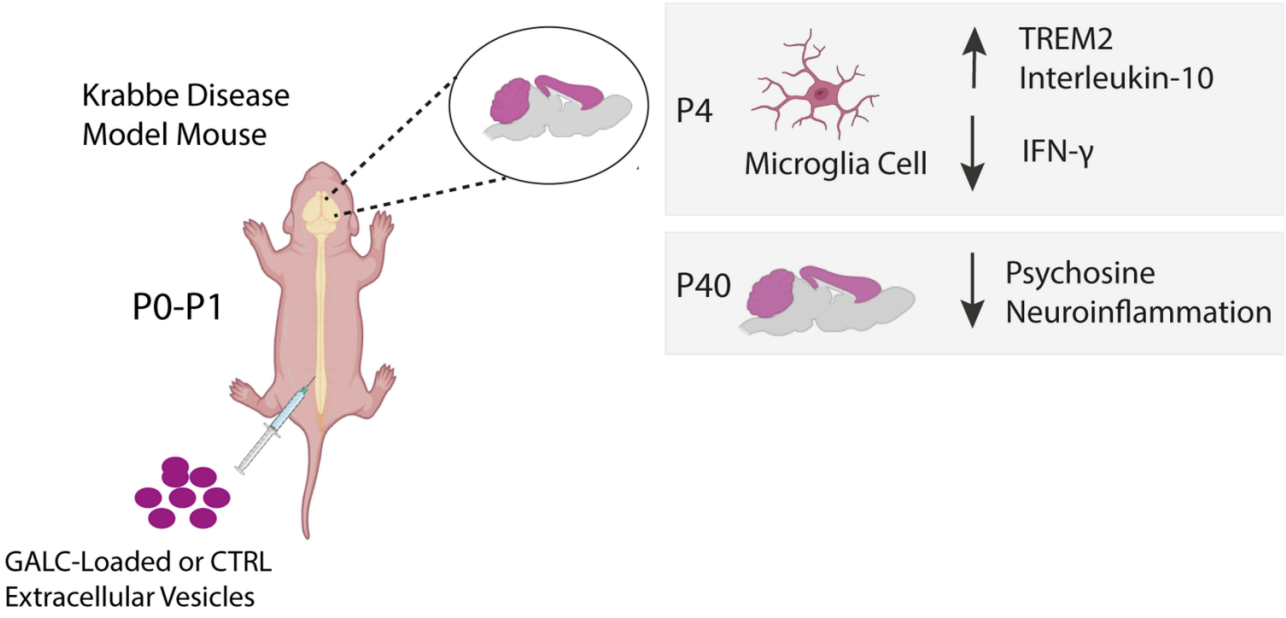


EVs delivered GALC to the brain, significantly reduced psychosine levels in the cortex and cerebellum in the Krabbe Disease (KD) mouse model.

EV-GALC therapy mitigated astrogliosis and shifted microglial activity toward an anti-inflammatory phenotype, with increased expression of IL-10 and TREM2.

Although EV-GALC treatment did not prevent demyelination or extend survival, it provides a proof of concept for using EVs in enzyme replacement therapy for KD, with potential as an adjunct to other long-term therapies.

mannose-6-phosphate receptor-mediated endocytosis.[9,10] This feature is crucial for correcting lysosomal storage deficiencies (LSDs) via enzyme replacement therapy (ERT). While ERT is effective for non-neuropathic LSDs, the inability of lysosomal enzymes to traverse the blood–brain barrier (BBB) limits its efficacy in LSDs with neurological involvement, such as KD.[10,11] The few studies using ERT with purified GALC enzyme in Twi mice clearly showed modest benefits, indicating that pure GALC enzyme might be of limited value to correct disease.[12] Moreover, recent findings further indicate that the transfer of GALC from one cell to another is inefficient,[13] reducing the benefits of using purified GALC enzyme for ERT. Recent studies successfully delivered GALC as cargo in carrier synthetic nanoparticles,[14,15] underscoring the possible therapeutic use of carrier-assisted delivery for GALC-ERT. However, the production of nanoparticles involves technical challenges, high costs, and many biodynamic aspects that remain unresolved.[16]

The goal of this study was to evaluate the effectiveness of a single neonatal delivery of therapeutic GALC using engineered extracellular vesicles (EVs) in triggering responses on cells from the central nervous system to mitigate disease manifestation in the neonatal Twi mouse. Our findings demonstrate that a single neonatal intrathecal administration of GALC-EV ERT reduced psychosine levels and weakened neuroinflammation in the Twi brain. Despite the absence of effects on demyelination and survival, these results underline the possibility of using EVs as a temporary intervention to alleviate central inflammation in KD, with possible applicability to other neuropathic LSDs.

# Materials and Methods

## Generation of HeLa and EV-GALC

A HeLa cell line (purchased from ATCC), expressing GALC was developed using an LV-GALC-HA construct with a neomycin resistance gene (Vector Builder Laboratories). The HeLa-GALC+ line maintains 100% GALC expression when supplemented with 400 μg/mL neomycin. Cells were maintained at low passage numbers (not beyond P10 and monitored on their morphology). Before EV collection, cells were grown with neomycin. At ~80% confluency, the media was replaced with fresh media without neomycin or serum and conditioned for 24 hours to collect EVs.

## EV Preparation

EVs were isolated from conditioned media of HeLa naïve and HeLa GALC cells using differential ultracentrifugation as previously described.[17] Briefly, after clearing large debris at 300xg for 5 min, the supernatant was sequentially centrifuged at 2,000 × g for 30 min, 12,000 × g, and 100,000 × g for 90 min each. Pellets were washed with PBS and centrifuged again at the same speeds. Medium-sized EVs were collected at 12,000 × g, and small-sized EVs, enriched in exosomes, at 100,000×g. All steps were done at 4°C, and EVs were stored at −80°C for further analysis.

## Nanoparticle Tracking Analysis (NTA)

The NTA analysis was conducted following our previously published protocol.[18] Briefly, EV particle size was measured using a NanoSight NS300. HeLa-derived EVs were diluted 500-fold in sterile PBS and introduced into a syringe connected to a pump attached to the instrument. For each sample, three videos were recorded using the NS300 software (v3.2) with the following settings: temperature 22.4–22.6°C, capture duration 30 sec/video, camera level set to 8, and detection threshold 7. Other capture settings included: laser type Blue-488, slider shutter: 317, slider gain: 15 and number of frames: 749.

## Mouse Glial Primary Cultures (MGPC) and EV Treatment

MGPCs were prepared from wild-type (WT) and Twi pups on postnatal (P) days 1–3.[19] Cortical cell suspensions from two pups were seeded onto 6-well plates and tissue culture flasks coated with 10 μg/mL poly-L-lysine, maintaining equal cell densities. The medium was replaced 4 days after plating. At 7 days in vitro (7 DIV), Twi MGPCs were treated with EV-GALC delivering a total of $2 \times 10^{-5}$ U of GALC activity (approximately 750 pmol/mg/h). GALC activity was measured in cell pellets collected 5 days after the initial treatment (12 DIV).

## Microglia Primary Culture (MPC), GALC Addition, and in vitro Stimulation

After 14 DIV, MGPC were shaken at 220 rpm and 37°C for 1 hour. Microglia from 2 mouse cortices were plated in a 6-well plate (~60% confluency). After 3 hours, some cultures received 2 nmol/mg/h of recombinant human GALC before collecting for RNA extraction. Microglia cells were also plated on coverslips to performed ICC analysis after 24hr in culture.

## Animals and Intrathecal Therapy Protocol

The animal procedures in this study were conducted in accordance with approved guidelines from the Animal Care (https://research.uic.edu/compliance/animal-care-use-acc/acc-forms-policies-guidelines/) and Use Committee at the University of Illinois at Chicago. WT and Twi neonatal (P0-P1) mice on a C57BL/6J genetic background were genotyped by PCR, as previously outlined.[20] Males and females were randomly selected in this work. Neonatal Twi mice (P0-P1) were treated with 13 μL of PBS, EVs naïve control (EV-CT) or EV-GALC, sourced from the same batch of EVs preparation. EVs + 1% trypan blue were administered via intrathecal (i.t.) delivery route at a dosage equivalent to ~3–4% of GALC activity in P1 WT mice (determined by empirical feasibility). All injections were carried out using a 29G insulin syringe (4428–1, Jelco/Smiths Medical ASD, INC., Keene, NH), inserted between the L5 and S1 vertebrae.

## Clinical Scoring and Tissue Collection

Clinical progression was assessed according to established protocols.[21,22] The scoring system ranged from 0 (no observable signs) to 5 (most severe neurological signs). Weekly assessments were conducted by an observer who was blinded to both, the genotype and treatment, starting from P20 until they reached the endpoint criteria. For the score, the following parameters were recorded: the weight lost (no change = 0; 0.1–0.5 g = 0.5; 0.6–1g = 1; 1.1–2g = 2); body tremor (none = 0; visible = 1); locomotion (normal = 0; waddling = 1; dragging limb = 1.5; paralyzed = 2) and wire grid hang latency (>45s = 0; 31s–45s = 0.5; 16s–30s = 1; 5s–15s = 1.5; <5s = 2). For tissue collection of this pilot study, three key time points were analyzed: P4 (close to the IT EV injection), P10 (intermediate, pre-myelination stage) and P40, the near the maximal survival of the Twi mice (post-myelination). At each time point, mice were sedated with isoflurane and transcardially perfused with PBS. Brain tissue was collected and divided into two halves: one half was immediately fixed in 4% paraformaldehyde (PFA) prepared in PBS for 24 hours, then equilibrated in sucrose in PBS, blocked, and sectioned for immunohistochemistry (IHC). The other half was dissected into three regions: cerebellum, cortex, and rest of the brain (without the cortex and cerebellum). The spinal cord was sectioned into cervical, thoracic, and lumbar segments. Also, liver, lungs, and sciatic nerve were collected. Tissues were immediately frozen for further analysis.

## GALC Activity

HeLa cells, EVs, MGPCs, and frozen tissue were homogenized in $H_2O$ containing Protease and phosphatase inhibitors cocktail PIC using a #VCX 130 sonicator (Sonics and Materials Inc., Newton, CT). Protein concentration of the samples was determined using the Pierce BCA kit (23225, Thermo Scientific). GALC activity was measured by incubating 10µg of lysates with the fluorescent substrate (6HMU-beta-D-galactoside) as described in.[22] Briefly, after 17 hours of incubation at 37°C, the reaction was stopped with a stop buffer (0.2 M glycine/NaOH, pH 10.7 + 0.2% Na-SDS + 0.2% Triton X-100). Fluorescence was measured at 370 nm/535 nm using a Beckman Coulter DTX 880.

## Acid Ceramidase Activity

Enzymatic assays were carried out following a previously established protocol.[23] Summarily, 10µg lysates were incubated with 0.2M sucrose, 25 mM sodium acetate buffer (pH 4.5), and 4 mM Rbm14-12 substrate at 37°C for 3 hours. The reaction was stopped with methanol and NaIO4 (2.5 mg/mL in 100 mM glycine/NaOH, pH 10.6), and fluorescence was measured after 2 hours in the dark at 37°C (370 nm/465 nm). Blanks excluded enzyme sources.

## Psychosine Analysis

Psychosine was extracted from 200 µg of tissue homogenates using methanol-acetic acid solution with Lactosyl-(β)-sphingosine (d18:1) (Avanti Polar Lipids, Alabaster, AL) as an internal standard. After 1 hour of incubation at room temperature, samples were centrifuged at 16,000 × g at 4°C, and supernatants were analyzed by liquid chromatography-tandem mass spectrometry. For the full protocol, refer to reference.[22]

## Immunofluorescence Analysis

For immunocytochemistry (ICC), primary cultures were fixed in 4% PFA-PBS for 20–30 min at room temperature. For immunohistochemistry (IHC) fixed brain tissue was cryoprotected in 20% sucrose and sectioned into 30- µm sagittal slices using a Leica CM3050 cryostat (Leica Biosystems). The floating sections or primary cell culture were washed 3 times with PBS and incubated overnight at room temperature with primary antibodies diluted in PBS containing 0.2% BSA, 0.1% Triton X-100. Primary antibodies used were anti-MBP (1:600, a gift from Dr Ernesto Bongarzone, University of Illinois at Chicago), anti-IL-10 (1:500, AF519, R&D Systems), Isolectin GS-IB4 Alexa Fluor 488 Conjugated (Invitrogene), anti-NeuN (1:800, D4G40, Cell signaling), anti-doublecortin (1:200, 4604S, Cell signaling), anti-Iba1 (1:800, 019–19741, Fujifilm), anti-CD68 (1:800, MCA1957, Biorad), anti-TREM2 (1:200, D8I4C, Cell signaling), anti-GFAP (1:800, AB5541, EMD Millipore), anti-PDGFRα (1:200, ab93531, Abcam), anti-GALC (1:50, in-house produced monoclonal IgG). For TREM2 antibody, tissue sections were pre-treated in 10 mM citrate sodium buffer, pH 6.0, at 100°C, 15 minutes for antigen retrieval. After three washes with PBS, secondary antibodies coupled to Alexa Fluor 488, 565, or 790 (1:1,000) were incubated for 2h at RT. After

being mounted with VECTASHIELD Antifade Mounting Medium with DAPI (H-1200-10, Vector Laboratories), the samples were imaged using confocal microscopy (Leica TCS SPE, Wetzlar, Germany). For quantitative analyses of GFAP and MBP immunostaining, confocal microscopy images were captured using consisted parameters across all groups, and the mean fluorescence intensity per field was analyzed by ImageJ. To determine the abundance per field of cells positive for CD68, or cells double-positive for CD68/TREM2 or IL-10/Iba1, confocal images were analyzed by ImageJ for each antibody using the Cell Counter plug-in. All analyses were conducted in a blinded manner with respect to the experimental condition and group.

## Western Blot Analysis

Lysates made in Milliq-water containing PIC were diluted in a 10X buffer solution (20 mM Tris-HCl pH 7.4, 1% Triton X-100,150 mM NaCl, 5nM $MgCl_2$) and 10–20 µg of proteins were loaded into 4–12% Bis-Tris Protein Gels, 1.5 mm (Invitrogen). After gel electrophoresis, proteins were transferred onto PVDF membranes (Bio-rad). Membranes were fixed overnight in methanol at RT, activated in methanol the following day, and blocked with 5% non-fat milk in TBS for 1 hour at RT. Primary antibodies were prepared in 1% BSA/TBS and incubated overnight at 4°C. Secondary antibodies, labeled with Licor IRDye of different isotypes were diluted in 5% non-fat milk/TBS-Tween (0.1%) + 0.01% SDS (1:10,000) and incubated for 1 hour at room temperature. Blots were washed and visualized on an Odyssey Fc Imaging system (LI-COR, Lincoln, NE). Primary antibodies used included: Alpha Tubulin (1:5,000, CP06, EMD Millipore), GFAP (1:700 AB5541, EMD Millipore); CD68 (1:500, ab303565, Abcam); MBP, a kind gift from Dr Bongarzone, University of Illinois at Chicago (1:700).

## Enzyme-Linked Immunosorbent Assay (ELISA) for TREM2 and IL-10

For TREM2 analysis (Mouse TREM2-Intracellular SimpleStep ELISA®, #ab314369), P10 lysates were prepared in 1x Cell Extraction Buffer PTR and PIC, centrifuged at 18,000 × g, and protein concentration determined by BCA. Samples concentrations were adjusted to 0.5 µg/µL with buffer PTR and 50 µL of each sample was loaded in Pre-Coated 96-well Microplate, following the indicated by the kit instructions. For IL-10 ELISA (IL-10 Mouse Elisa kit, #ab108870), cortices were processed with PBS containing 1% Tx-100 and PIC, centrifuged at 14,000 × g for 20 minutes. Sample concentration was diluted to 0.5 µg/µL with Diluent N, and 50 µL of the sample was loaded into IL-10 Microplate, according to the manufacturer instructions. Protein levels were measured in a plate reader at 450 nm, and the concentrations (pg/mL) were determined using a TREM2 or IL-10 standard calibration curve, respectively.

## Isolation of RNA and Quantitative RT-PCR (RT-qPCR) Analysis

RNA was isolated using TRIZOL reagent (Invitrogen) following the manufacturer's instructions. RNA concentration and purity were assessed using NanoDrop spectrophotometer (ND-100). cDNA synthesis was carried out using RevertAid ® H Minus M-MuLV reverse transcriptase enzyme (Perkin Elmer, Waltham, MA, USA) according to the manufacturer's protocol. Negative controls were performed in parallel without the reverse transcriptase enzyme. RT-qPCR reaction was performed using iTaq Universal SYBR Green Supermix (Cat# 1725121, Bio-Rad) on a Real-Time PCR Detection System (Bio-Rad, USA). Calibration and efficiency curves of set of primers were established with serial dilutions. Reactions were conducted in duplicates, and mRNA was normalized to GAPDH as reference gene. Relative expression was calculated and plotted using the $2^{-\Delta\Delta Ct}$ method. Primers used for qPCR are listed in Supplementary Table 1.

## Statistics

Data were analyzed by Student's *t*-test or one-way ANOVA followed by Tukey or Šidák post-hoc test, considering a $p < 0.05$ value as statistically significant. Results are given as the mean ± standard error of the mean (SEM). All analyses were performed with GraphPad Prism version 10.1.1 (270) (La Jolla, CA, USA).

# Results

## GALC-Enriched EVs Transfer Active Enzyme and Correct GALC Deficiency in Cultured Twi Cells

HeLa cells were transduced with a lentiviral vector to express murine GALC enzyme tagged with hemagglutinin (HA) prior to isolation of EVs (Figure 1A). Particle size analysis by NTA confirmed the presence of ~200nm size EV (Figure 1B), and GALC presence in these particles was verified by immunodetection of the HA tag (Figure 1C). GALC activity in EVs showed a ~15-fold increase compared to controls (Figure 1D). A positive correlation between EV-GALC protein concentration and enzymatic activity was observed (Figure 1E). To test the efficacy of EVs to transfer therapeutic enzyme, mouse glial primary cultures (MGPCs) from Twi and wild-type (WT) pups were prepared and incubated with EVs from control and GALC-expressing cells. Treatment of Twi cells resulted in a ~1.5-fold increase in GALC activity respect to non-treated Twi cells (Figure 1F) and an ~80% reduction in psychosine levels (Figure 1G), demonstrating a significant capacity of EVs to transfer corrective GALC enzyme.

## GALC ERT Following a Single Neonatal Intrathecal Delivery of EV-GALC Reduces Psychosine Levels in the Cortex and Cerebellum of Twi Mice

We tested the capacity of EVs to deliver active GALC in vivo. For this, Twi mice pups were administered with a single IT injection of EV-GALC (~$1.2 \times 10^9$ EVs) or PBS (vehicle) on P1 and euthanized at either P4, P10 or P40 (experimental

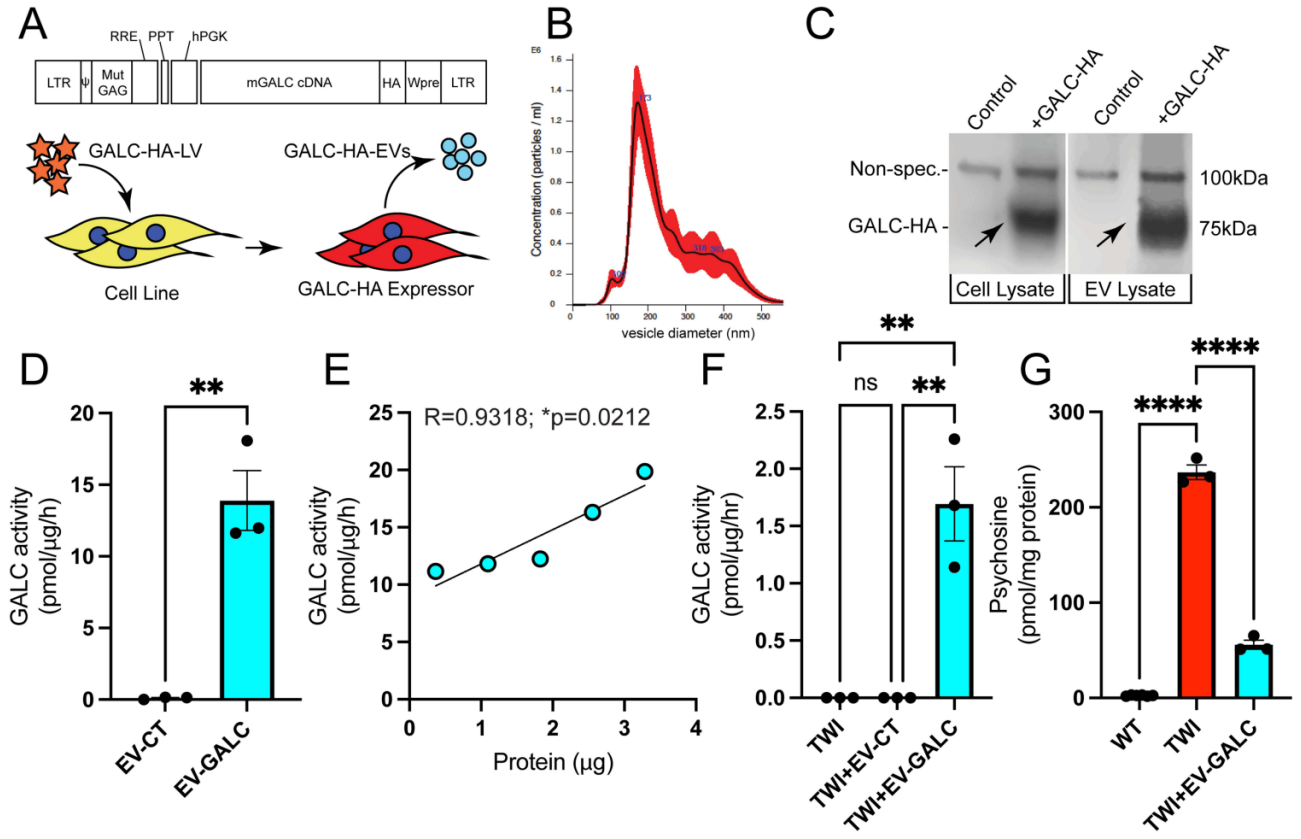


**Figure 1** Characterization of HeLa EVs expressing GALC. (**A**) Diagram representing the experimental approach to generate EVs expressing GALC (HeLa-GALC-HA). (**B**) Representative plot obtained from the analysis of the EV-GALC population obtained after 100,000xg centrifugation by nano site scatter analysis displays that most of EVs are in the range of 200nm. (**C**) Cells and EVs lysates were immunoblotted using antibodies anti-GALC. A ~75kDa band was detected in the lysates from lysates obtained from HeLa-GALC-HA (arrows) but not in HeLa control lysates. (**D**) GALC enzymatic fluorometric assay was performed on lysates obtained from control EVs (EV-CT) or EVs loaded with GALC-HA (EV-GALC). n=3 per condition. ** $p < 0.01$ (*t*-test). (**E**) Correlation between GALC activity and the concentration of proteins employed from EV-GALC-HA. The amounts of protein assayed were: 0.5; 1.0; 1.8; 2.5 and 3.2 µg, R = 0.9318; *p = 0.0212. (**F**) GALC activity assays were performed in lysates obtained from Twi MPGCs that were treated with control (TWI+EV-CT) or GALC-loaded EVs (TWI+EV-GALC) for 7 days. (**G**) Psychosine levels were analyzed in WT, Twi, and Twi MPGCs treated with EV-GALC. Data was obtained from three independent cultures per condition. ** $p < 0.01$; **** $p < 0.0001$ (one-way ANOVA, followed by Tukey´s post-hoc test).

approach diagram, Figure 2A). Measurement of GALC activity in total brain showed detectable and significant levels of GALC activity above Twi background at P10 but not at P40 (not shown), results that were expected due to the transient administration of GALC. Regional analyses showed that GALC activity was distributed to various regions of the P10 EV-GALC treated Twi brain with significant increases with respect to non-treated Twi in the cortex (Figure 2B). The level of GALC in EV-GALC treated TWI represent ~3.8% of a WT in the cortex (WT 2.1± 0.28 pmol/g/hour vs TWI EV-GAL 0.08 ± 0.0097 pmol/g/hour). Non-significant increases of GALC were recorded in the cerebellum (Figure 2D), and in the rest of the brain (Figure 2F). In the spinal cord, enzyme activity was significantly increased only in the thoracic segment (Figure 2H) but not in lumbar and cervical regions (Figure 2H). Interestingly, we detected significant reductions

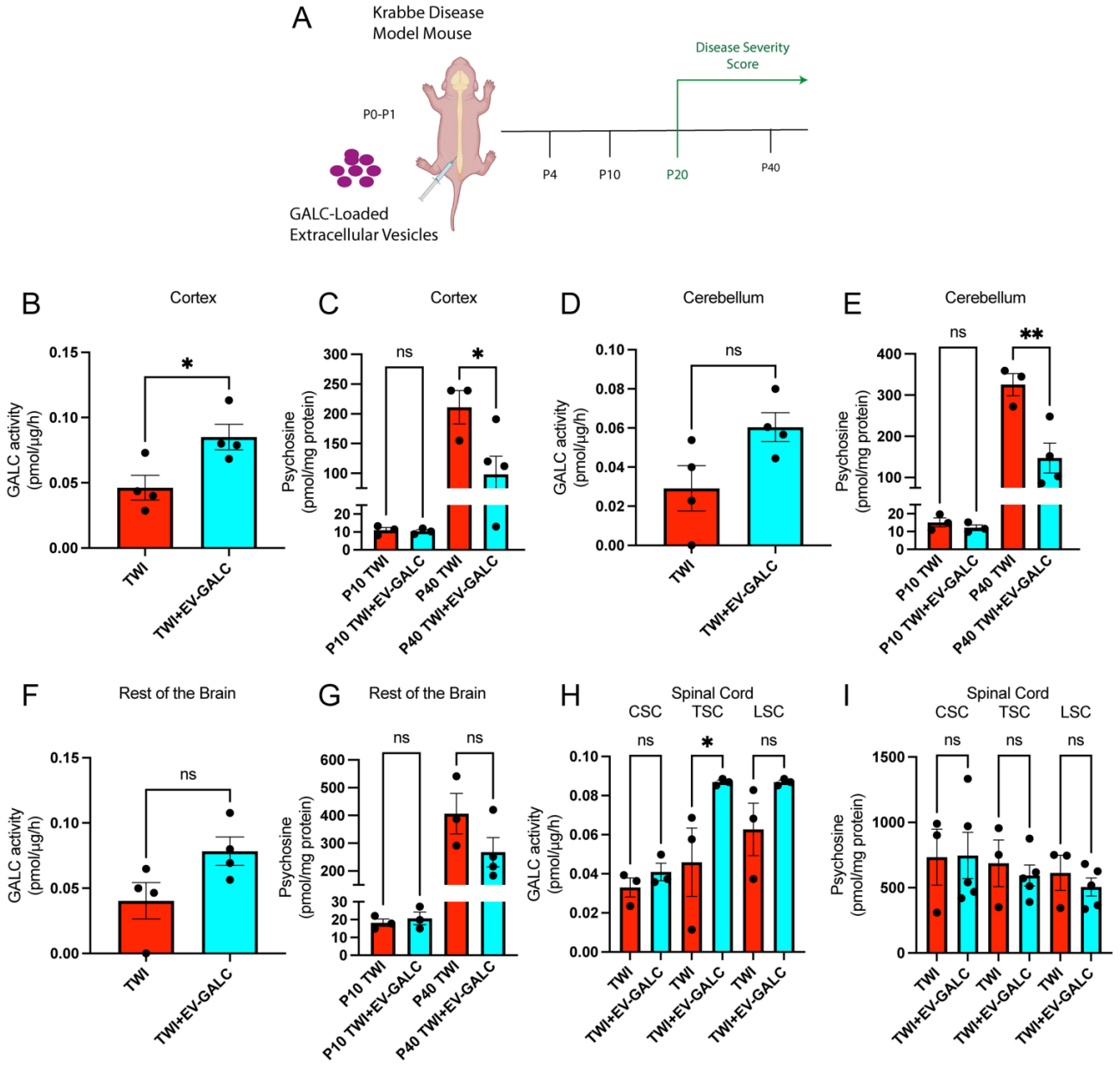


**Figure 2** Single neonatal intrathecal delivery of EV-GALC reduces psychosine levels in the cortex and cerebellum of Twi mice. (**A**) Experimental approach diagram. Briefly, newborn Twi mice received a single i.t. injection of EV-GALC or EV-C at postnatal day 0–1 (P0-P1) and then collected at P4, P10 or P40 time points for analysis. Clinical score was assessed from P20 until P40, the maximal survival of the twitcher mouse. (**B**) Tissues were collected at P10, and GALC activity was assayed in the cortex, (**D**) cerebellum, (**F**) rest of the brain and (**H**) spinal cords, including cervical (CSC), thoracic (TSC) and lumbar (LSC) regions (N= 4 animals per condition). * $p < 0.05$; ns: $p > 0.05$ (*t*-test). (**C**) Psychosine levels were analyzed at P10 and P40 in different regions of brain, including cortex, (**E**) cerebellum, (**G**) rest of the brain, and (**I**) spinal cords (cervical, thoracic and lumbar regions) from control Twi or Twi mice treated with EV-GALC. Graphs represent the mean ± SEM from 3–4 animals per condition. ** $p < 0.01$; * $p < 0.05$; ns: $p > 0.05$ (one-way ANOVA followed by Šidák post-test).


https://doi.org/10.2147/IJN.S523938

of psychosine in the cortex (Figure 2C), and cerebellum (Figure 2E) of P40 but not P10 Twi treated mice. Psychosine remained largely unchanged in the rest of the brain (Figure 2G) and spinal cord (Figure 2I and Supplementary Figure 1A). GALC activity in peripheral nerves, liver, and lung remained at TWI levels (not shown) with no significant effects on psychosine levels at either P10 (Supplementary Figure 1B) or P40 (Supplementary Figure 1C). As expected, injection of control EVs without GALC (EV-CT) did not change significantly GALC activity and the high levels of psychosine with respect to untreated Twi mice (Supplementary Figure 1D–E). Measurement of the activity of acid ceramidase (ASAH1), the enzyme involved in most psychosine synthesis in the context of TWI mice, showed no significant changes in the cortex and cerebellum brain regions or time point of our study, but only between WT and Twi +EV-GALC in the rest of the brain at P10 (Supplementary Figure 2).

## Neonatal ERT with EV-GALC Ameliorates Gliotic Inflammatory Responses Without Major Impact in Demyelination and Survival of Twi Mice

Based on our findings of reduced psychosine levels in the P40 Twi brain, we examined whether this reduction of psychosine was accompanied by improved neuropathology. Immunohistochemical analysis was done on brain sections for Cluster of Differentiation 68 (CD68, microglia), Glial Fibrillary Acidic Protein (GFAP, astroglia), and myelin basic protein (MBP, myelin). Our results showed a visible reduction of astrogliosis (Figure 3A–C) and microgliosis (Figure 3E–G) in the cortex of Twi mice treated with EV-GALC with respect to untreated Twi. Background controls for these analyses are shown in Supplementary Figure 3. Quantitative analyses showed significant reductions of GFAP+ and CD68+ signals in treated Twi vs untreated Twi (Figure 3D and H). In contrast, myelination appeared unchanged in treated Twi brains with respect to low levels detected in untreated Twi, which was significantly lower than WT brains (Figure 3I–L and O). Western blot analyses showed similar lowering trends for GFAP+ cells and CD68+ cells in the cortex of treated Twi mice although without reaching significance (Figure 3M, N and Supplementary Figure 4). As expected, injection of control EVs did not change significantly the high levels of gliotic responses (Supplementary Figure 5A–F).

Despite amelioration in inflammatory gliosis and psychosine metabolism, we did not observe significant differences in disease progression between experimental groups (Supplementary Figure 6A–E). Immunohistochemical analysis at P4 detected that GALC protein driven from EVs was uptaken primarily by microglia (Figure 4D and H arrows), blood vessels (Figure 4L, arrows) but not in astrocytes (Figure 4P) and to a much lesser extent, in oligodendrocyte progenitor cells (Supplementary Figure 7D, arrows) and neurons (Supplementary Figure 7H–L). Due to the introduction of a nonsense codon, no GALC protein is produced in the Twi mice, as shown in the immunohistochemical analysis performed using anti-GALC in Twi tissue, no GALC immunoreactivity was observed (Supplementary Figure 7Q–S). The specificity of the secondary antibodies was additionally verified (Supplementary Figure 7M–P). Together, these findings show that ERT for GALC using EV-assisted delivery effectively increased GALC activity and reduced psychosine accumulation in some CNS regions, with the greatest impact observed in the cortex of Twi EV-GALC-treated mice.

## Lower Inflammation Was Associated with Anti-Inflammatory Cytokines

To investigate the mechanisms through which treatment with EV-GALC reduced inflammation in the Twi cortex, we conducted a comprehensive gene expression screening of key anti-inflammatory mRNAs by RT-qPCR on the P10 experimental groups. Analyses included cytokines IL-4, IL-6, IL-10, IFN-γ, TNF-α, and MCP-1. Additionally, we examined the expression of three critical molecules involved in modulating the immune response in the nervous system: TREM-2 (Triggering Receptor Expressed on Myeloid Cells 2), essential for microglia activation, BDNF (brain-derived neurotrophic factor) associated with anti-inflammatory roles, and NOS2 (Nitric Oxide Synthase 2), which participate in pro-inflammatory responses. We found that EV-GALC-treated Twi mice showed a significant increase in the brain expression of IL-10, TREM-2, and BDNF compared to naïve Twi mice (Figure 5). Additionally, IFN-γ showed a significant reduction in the brain of EV-GALC-treated Twi mice compared to naïve Twi mice (Figure 5). The altered expression of cytokines was not observed when Twi received EV-CT (Figure 5, blue bars). There were no significant differences in the levels of TNF-α, IL-4, and IL-6 except for MCP-1 (Supplementary Figure 8A). Other genes, such as

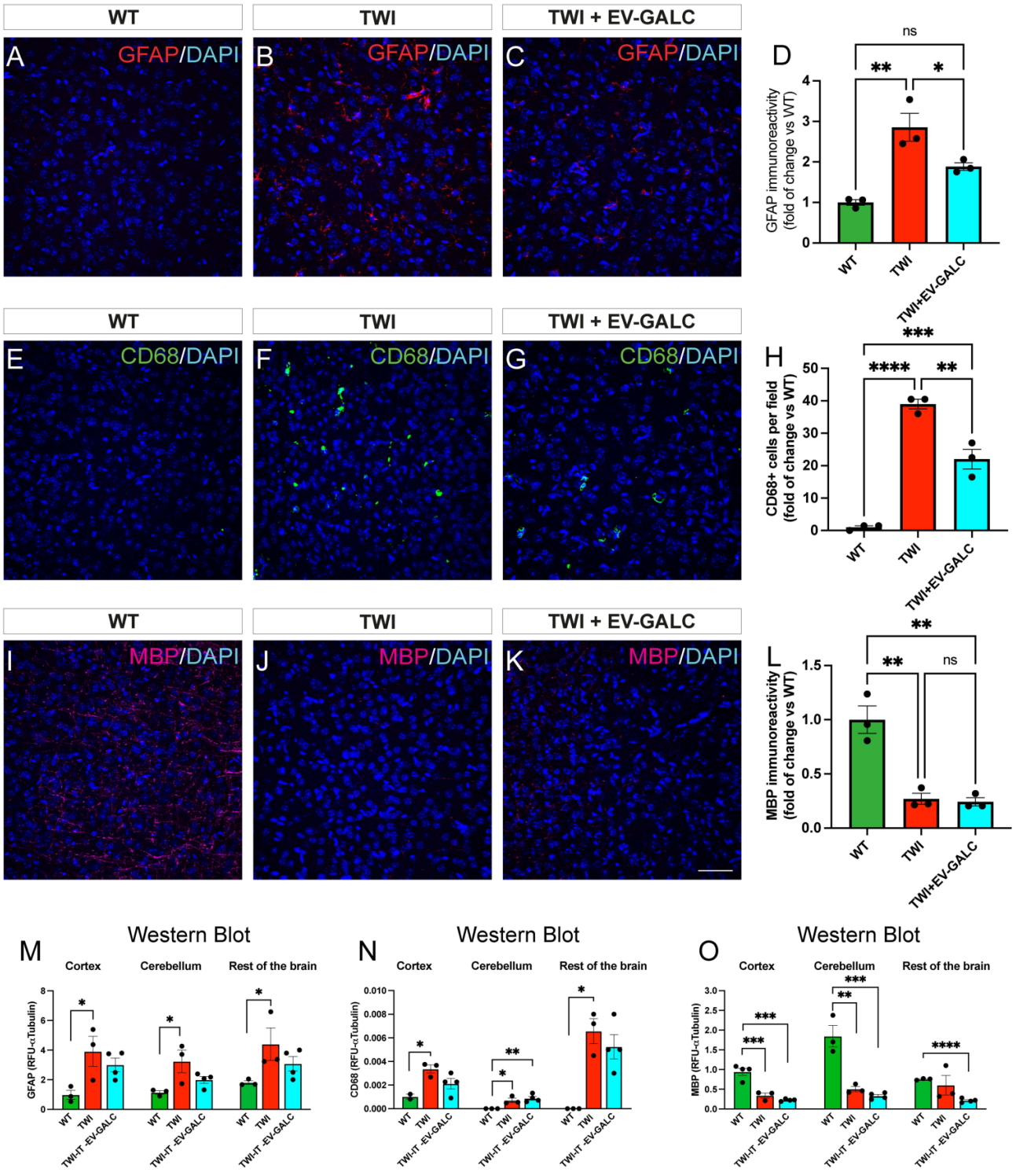


**Figure 3** Analysis of microgliosis, astrogliosis and demyelination in the brain of Twitcher mice treated with EV-GALC. Representative confocal images obtained from immunohistochemistry analysis of **(A-C)** GFAP (red), (**E–G**) CD68 (green) and (**I–K**) MBP (magenta) in the cortex of P40 WT, Twi or Twi mice treated with EV-GALC. Nuclei were stained with DAPI (blue). Scale bar: 25 µm. (**D**) The fluorescence intensity of GFAP, (**H**) the number of CD68+ cells per field, and (**L**) fluorescence intensity of MBP were quantified in the cortex of WT, Twi and Twi EV-GALC. Graphs represent the mean ± SEM for the fold of change with respect to WT. 3 slides were analyzed per animal. n = 3 animals per experimental condition. **** $p < 0.0001$; *** $p < 0.001$; ** $p < 0.01$; * $p < 0.05$; n.s: $p > 0.05$ (one-way ANOVA). (**M–O**) Western blot analysis of (**M**) GFAP, (**N**) CD68 and (**O**) MBP from lysates obtained from the cortex, cerebellum and rest of the brain of P40 WT, Twi or Twi mice treated with EV-GALC at P1. Quantification of MBP, CD68 or GFAP levels were normalized against the levels of α-tubulin. Graphs represent the mean ± SEM obtained from 3–4 animals per condition. * $p < 0.05$; ** $p < 0.01$; *** $p < 0.001$. (one-way ANOVA followed by Tukey´s post-test).


https://doi.org/10.2147/IJN.S523938

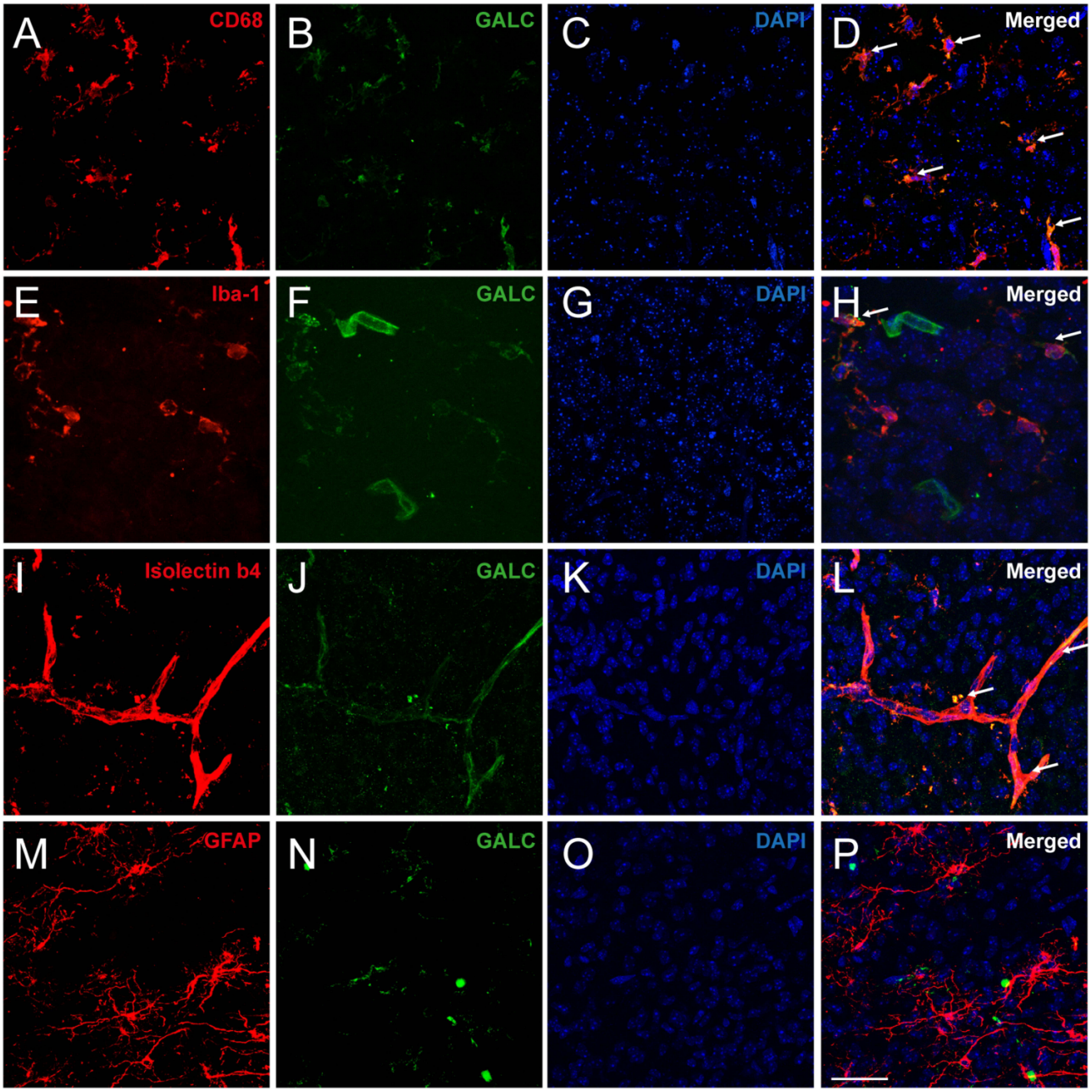


**Figure 4** Confocal microscopy analysis of EV-GALC biodistribution in the brain of Twi mice. Immunohistochemical analyses were performed in brains from P4 Twi mice treated with EV-GALC using (**B, F, J** and **N**) anti-GALC (green) along with different cells markers, including (**A**) CD68 (red), (**E**) Iba-1 (red), (**I**) Isolectin B4 (red) and (**M**) GFAP (red) in order to identify the cell-specific distribution of EV-GALC. Representative confocal microscopy images are shown of data obtained from 3 animals per experimental condition. Nuclei were stained with DAPI (blue). Colocalization is shown in (**D,H,L** and **P**) with arrows. Scale bar: 25 µm.

Lamp1 (Lysosomal Associated Membrane Protein 1), which supports an anti-inflammatory environment by maintaining lysosome function, and MMP9 (Matrix Metalloproteinase-9) typically associated with pro-inflammatory effects and tissue damage showed no significant differences across groups (Supplementary Figure 8A).

To assess whether protein expression of TREM-2 and IL-10 correlated with our mRNA results, we performed immunohistochemical analyses in cortical sections of P4 brains and ELISA assays in P10 brain extracts from each experimental group. Our results confirmed an increase in TREM-2 protein expression in CD68+ microglia in the Twi cortex following treatment with EV-GALC (Figure 6I–L) over levels observed in controls groups (Figure 6A–H), reaching statistical significance (Figure 6M). Likewise, ELISA quantification showed significant increases of TREM-2

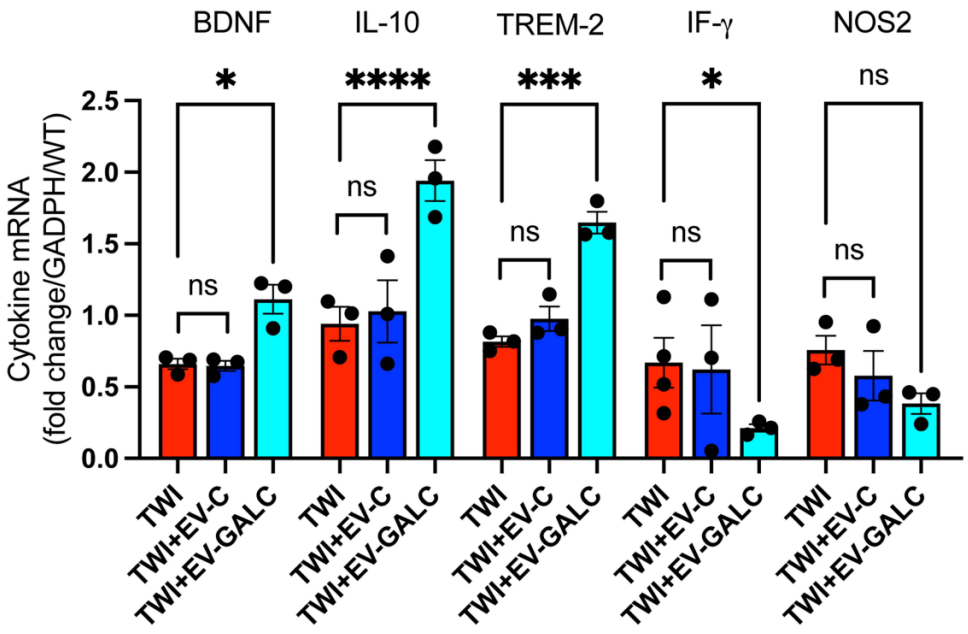


**Figure 5** Modulatory effects of EV-GALC in the expression of pro- and anti-inflammatory cytokines in the cortex of Twi mice. RT-qPCR analyses were performed from the RNA obtained from cortices of P10 WT, Twi or Twi treated with EV-C or EV-GALC for: BDNF, IL-10, TREM-2, IFN-γ and NOS2. The fold of change in mRNA expression for every gene was normalized against the expression of GAPDH. Values are represented as a fold of change against the WT condition. Graphs represent the mean ± SEM obtained from 3 animals per condition. * $p < 0.05$; ** $p < 0.01$ (*t*-test).

in the cortex of Twi mice treated with EV-GALC (Figure 6N) as well as in other areas of the brain (Supplementary Figure 8B). Similarly, there was an increased expression of IL-10 in cortical microglial cells (Figure 7I–L) over levels observed in controls groups (Figure 7A–H), reaching statistical significance (Figure 7M). IL-10 protein levels were also increased in cortical extracts from EV-GALC-treated mice (Figure 7N). Other areas such as the cerebellum did not show significant changes in IL-10 levels (Supplementary Figure 8C). The significant increase of IL-10 and TREM-2 measured in the cortex upon EV-GALC were not observed in EV-C treated mice (Supplementary Figure 8D–E), indicating that GALC rather than EVs are promoting IL-10 and TREM-2 upregulation in microglia.

These results suggest that a reduction in inflammation in the Twi cortex after ERT with EV-GALC involved at least TREM-2 and IL-10. To further investigate this, we isolated microglial cells from brain cortices of WT and Twi pups and ERT-treated them with recombinant GALC enzyme. RT-qPCR analyses showed significant increases of TREM-2 mRNA (Figure 8A) and non-significant increases of IL-10 mRNA (Figure 8J). Immunocytochemical analyses confirmed these findings for both TREM-2 and IL-10 (Figure 8B–I and K–R).

Being IL-10 an anti-inflammatory cytokine regulating microglial activation, and TREM-2 promoting the activation and polarization of microglia towards an anti-inflammatory phenotype, altogether, our results suggest that treatment of Twi pups with an early ERT via EV-GALC infusion modulates the inflammatory response by enhancing anti-inflammatory pathways and reducing specific pro-inflammatory signals.

## Discussion

This is the first proof of concept study to provide evidence that EVs are capable of delivering active GALC enzyme to the brain and to successfully reconstitute enzyme activity to decrease toxic levels of psychosine in the Twi model of KD. As expected from our study, a single intrathecal neonatal infusion of EV-GALC did not prevent demyelination or significantly modified disease milestones in Twi mice (Supplementary Figure 6). However, the modest increase in GALC activity ~3–4% of GALC levels of the WT brain was sufficient to impact in a significant reduction of ~40% in psychosine levels in the Twi cortex and cerebellum with respect to untreated Twi controls (Figure 2). Therefore, further studies, including scaling up EV-GALC doses or targeting specific neural cell types in Twi mice, may provide greater protection against inflammation and demyelination.


https://doi.org/10.2147/IJN.S523938

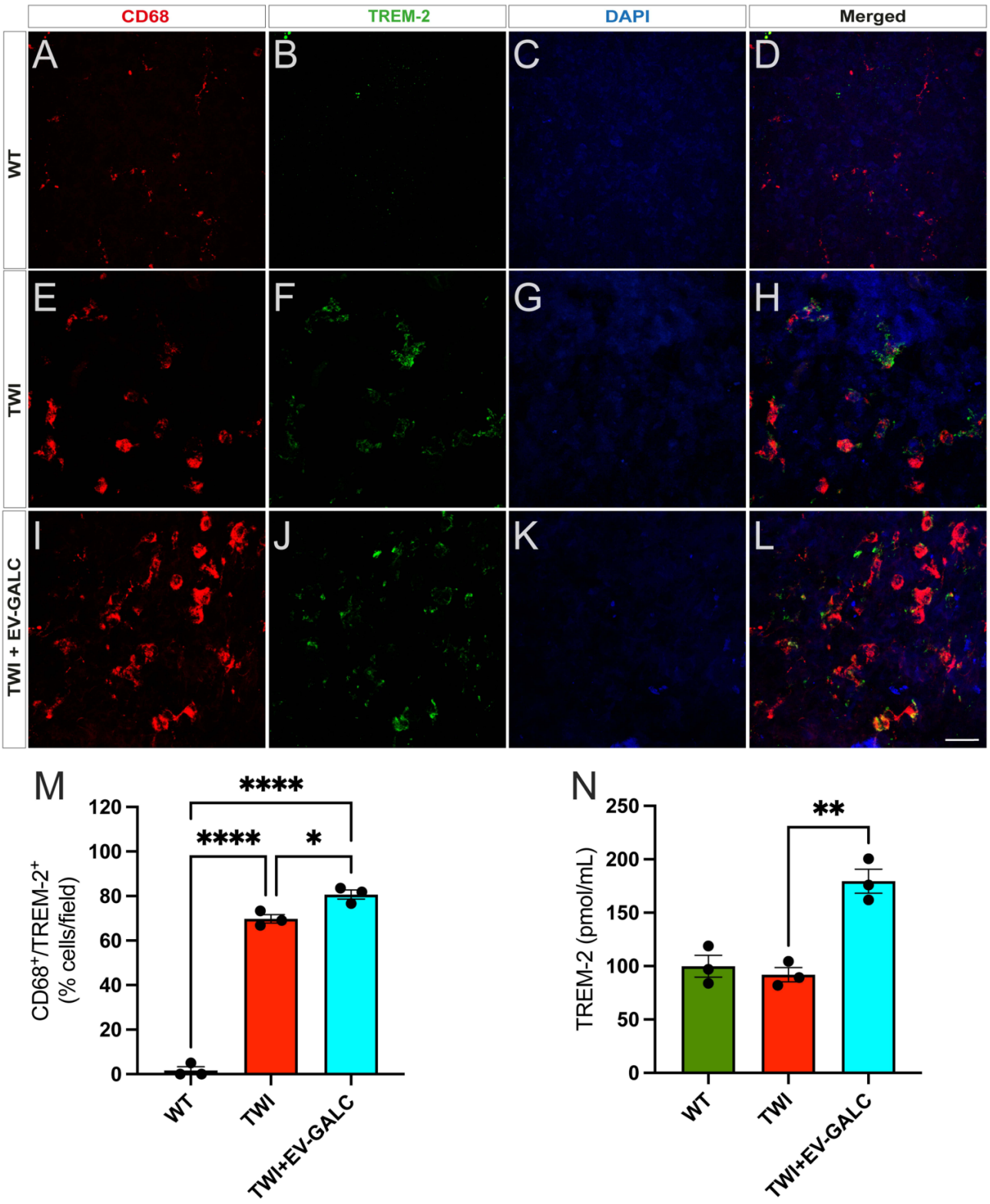


**Figure 6** TREM-2 is upregulated in microglia of Twi mice treated with EV-GALC. (**A–L**) Immunohistochemistry analyses were performed in the brains of P4 WT, Twi, and Twi mice treated EV-GALC, using (**A, E** and **I**) CD68 (red) and (**B, F** and **J**) TREM2 (green). Nuclei were stained with DAPI (blue). Representative confocal images from the cortex are shown for each antibody along with the merged images. Scale bar: 25 µm. (**M**) The percentage of CD68+ cells that were also positive for TREM-2 (CD68 +/TREM-2+) was quantified for each condition (3 slices per animal, 3 animals per condition). (**N**) ELISA for TREM-2 was performed in lysates obtained from the cortex of P10 WT, Twi and Twi mice treated with EV-GALC at P1. Graphs represent the mean ± SEM obtained from 3 animals per condition. * $p < 0.05$; ** $p < 0.01$; **** $p < 0.0001$ (one-way ANOVA followed by Šidák post-test).

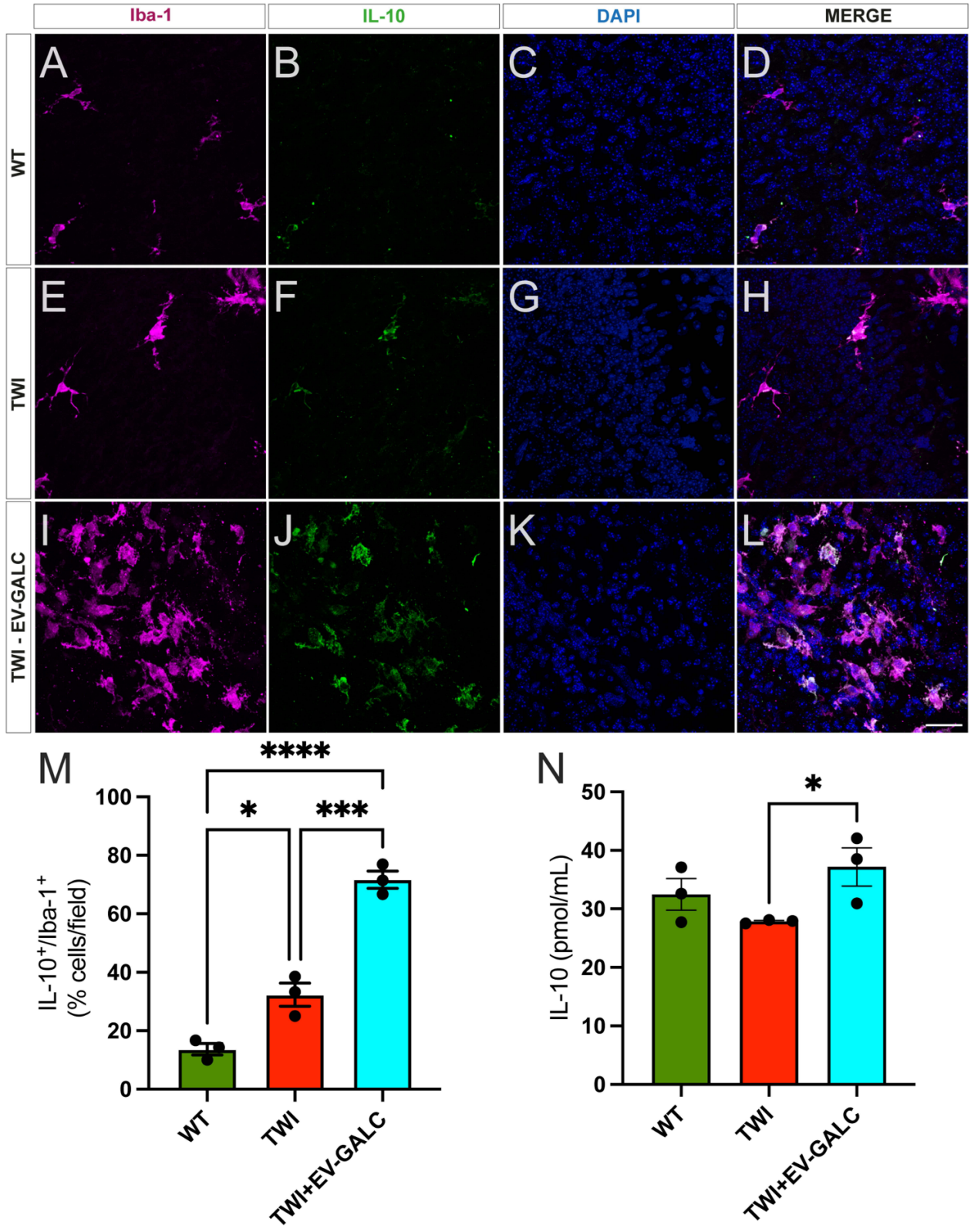


**Figure 7** IL-10 is upregulated in microglia of Twi mice treated with EV-GALC. (**A–L**) Immunohistochemistry analyses were performed in the brains of P4 WT, Twi, and Twi mice treated with EV-GALC, using (**A, E, I**) Iba-1 (magenta) and (**B, F, J**) IL-10 (green). Nuclei were stained with DAPI (blue). Representative confocal images from the cortex are shown for each antibody along with the merged images. Scale bar: 25 µm. (**M**) The percentage of Iba1+ cells that were also positive for IL-10 (IL-10+/Iba1+) was quantified for each condition (3 slices per animal, 3 animals per condition). (**N**) ELISA for IL-10 was performed in lysates obtained from the cortex of P10 WT, Twi and Twi mice treated with EV-GALC at P1. Graphs represent the mean ± SEM obtained from 3 animals per condition. * $p < 0.05$; *** $p < 0.001$; **** $p < 0.0001$ (one-way ANOVA followed by Šidák post-test).


https://doi.org/10.2147/IJN.S523938

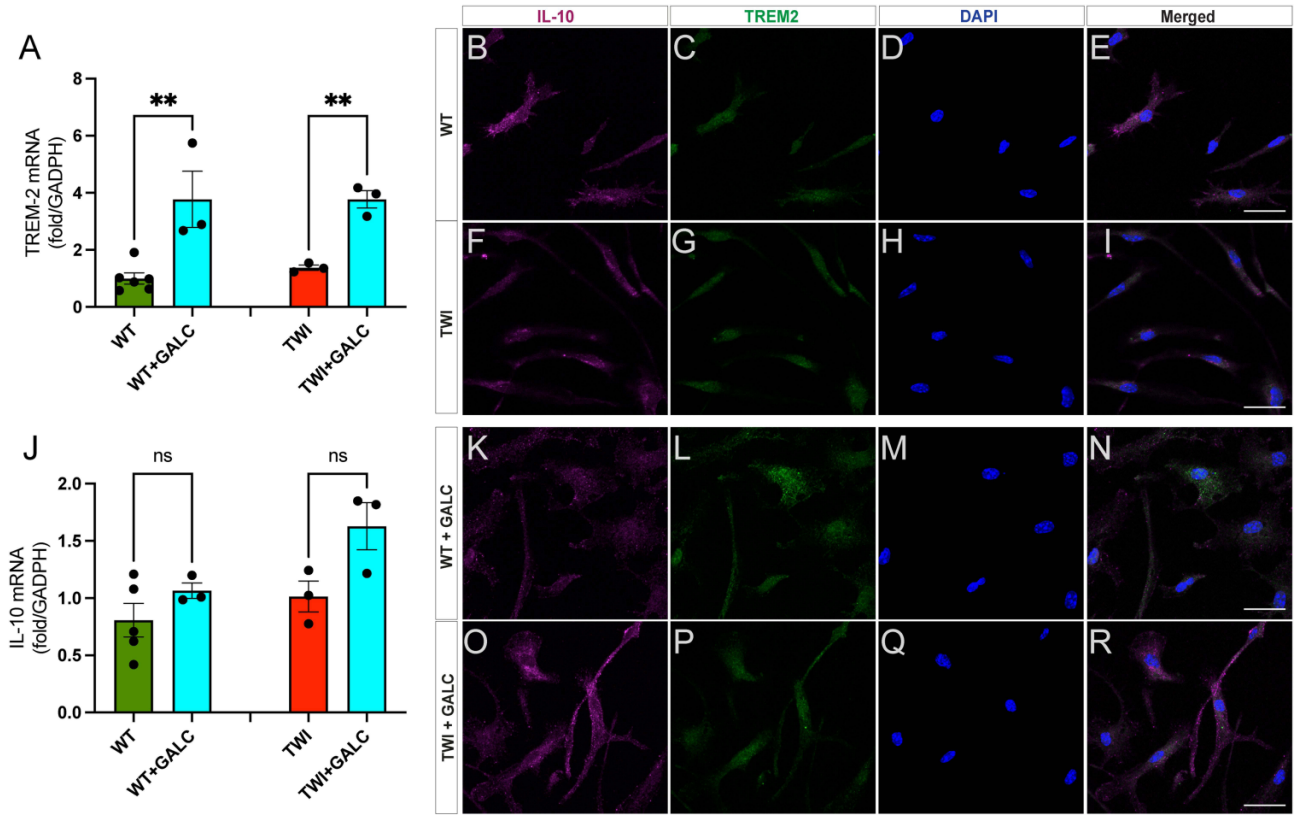


**Figure 8** Microglial cells up-regulate the expression of TREM-2 upon GALC treatment. (**A, J**) 14 DIV mouse microglial cultures obtained from WT or Twi mice were subjected to treatment with recombinant GALC (+GALC) and the expression profile of different mRNAs were analyzed. The genes analyzed included (**A**) TREM-2 and (**J**) IL-10. Graphs represent the mean ± SEM obtained from 3 independent cultures per condition. **p < 0.01; n.s: p > 0.05 (one-way ANOVA followed by Šidák post-test). (**B–R**) Immunocytochemistry analyses of 14 DIV mouse microglial cultures obtained from WT or Twi without or subjected to the treatment with recombinant GALC mentioned above using (**B, F, K** and **O**) IL-10 (magenta), or (**C, G, L** and **P**) TREM2 (green) antibodies. Nuclei were stained with DAPI (blue). Images were subsequently acquired by confocal microscopy. Scale bar: 25 µm.

Although levels of GALC were not therapeutic in our study, their effects on neuropathology were measurable and resulted in an improvement of astrogliosis and microgliosis, especially in cortical areas of the brain (Figure 3). The goal of this study was not to persistently provide GALC or prolong the lifespan of Twi mice, but rather to evaluate the protection of a transient input of GALC in the CNS ("buffer therapy") to decrease the built up of psychosine levels and neuroinflammation at neonatal life, a therapeutic window of time when GALC is needed right after a newborn diagnosis and before other treatments, such as BMT, are provided.

In general, while ERT facilitates reconstitution of the deficient lysosomal enzyme in peripheral tissues, its capacity to correct lysosomal deficiencies in the CNS is largely limited due to the presence and the filtering function of BBB. Thus, traditional ERT approaches for neuropathic LSDs are not practical. Few attempts were carried over to treat KD via ERT in KD mouse models, with all effectively resulting in insufficient replacement to prevent/stop the development of major pathological hallmarks.[12,24,25] The use of carriers such EVs to deliver enzyme across cell barriers is thought to facilitate the entry of lysosomal enzymes across the BBB into the CNS. EVs have demonstrated potential in delivering therapeutic agents in various LSDs[26,27] as well as in other conditions, including cancer, neurodegenerative disorders, and diabetes[28–30] and help reducing inflammation.[31] Ongoing clinical trials in cardiovascular diseases, cancer, neurodegenerative disorders, and COVID19 related acute respiratory distress (NCT01668849, NCT01159288, NCT03857841, NCT03384433. NCT05354141) further support their therapeutic potential.[32–34] These examples highlight the growing recognition of EVs as promising vehicles for the delivery of therapeutic cargoes, underscoring their possible clinical use. Our research contributes to this growing body of evidence by demonstrating for the first time the effectiveness of EVs in delivering GALC enzyme in the brain of a KD mouse model and suggests that an early ERT for GALC correction using EVs, while

evidently transient, exerts significant and lasting positive effects in some aspects of the pathology and metabolic blockage in the KD brain during early postnatal life.

The current standard of care for KD patients is HSCT, effectively reducing disease progression for a significant number of years when administered to asymptomatic or minimally symptomatic KD infants. However, most clinical results show that HSCT therapeutic benefits are largely exhausted by the teen years in most transplanted patients. Among the many factors influencing the long-term efficacy of HSCT, the delay between diagnosis, the transplantation procedure itself, and the starting of HSCT-derived corrective effects is crucial. This lag of time may take several weeks to a few months during which neuropathology continues to progress, further damaging the nervous system and limiting HSCT efficacy.[7,35] AAV-based gene therapy has also proved effective in animal models of KD; however, its current application on ongoing clinical trials were recently suspended. AAV-gene therapy should have a shortened delay between diagnosis and improvements in clinical readouts, but it also requires a few weeks to reach therapeutic effects. Therefore, despite their more limited therapeutic effects, adjunct treatments such as ERT using EV-GALC may provide significant protection during early postnatal life until long-term therapies such as HSCT are administered to the patients. Our small-scale study offers the proof of concept that EVs serve the purpose of rapidly delivering therapeutic GALC enzyme to the KD brain. Scalability, dosage, enzyme concentration, and EV-cell factories are aspects that would require dedicated refinement before clinical considerations.

It is not clear why the effect of EV-GALC treatment was limited mainly to the cortex and the cerebellum. At this moment, we speculate that the IT route of delivery might have contributed to this fact. After the IT injection, there is an immediate trypan blue staining first at the cerebellum and olfactory bulb. Our study suggests that the cortex is the primary region of the brain to show EV-GALC-derived benefits (Figure 2A and B). This is particularly relevant given the cortex's role in higher cognitive functions and memory processes, which underscores the importance of preserving its integrity. Supported by our IHC analysis, EVs were capable to deliver immunodetectable GALC primarily to microglial cells throughout the cortex and particularly those located near the meninges and in the brain parenchyma across the intercellular space. We did not detect significant levels of GALC enzyme in other cell types such as oligodendrocytes, neurons or astrocytes (Figure 4 and Supplementary Figure 7), which may be due to a poor uptake of EVs, a higher turnover of the enzyme, and/or the limit of immunodetection of GALC in these cells. At this moment, the cellular mechanism behind these microglia selective uptake is unknown, but previous studies suggest that microglial cells are the primarily cells that incorporate EVs upon LPS stimulation or when plasma EVs are injected in the brain.[36]

Our results show that the early GALC reconstitution brought a carry-over effect on reducing psychosine levels, most noticeable during the sick stage of the disease in the Twi mouse (Figure 2B, D, F and H).

At this moment, the reduction of psychosine levels may indicate changes in the anabolism of psychosine in the brain following ERT with EV-GALC. In view of the absence of significant changes in ASAH1 activity (key for psychosine synthesis; Supplementary Figure 2) in the brain, we hypothesize that changes in the metabolic profile of brain cells led to less synthesis. In this regard, our study demonstrated that proinflammatory Twi microglial cells underwent a shift towards anti-inflammatory microglia. KD presents significant inflammatory components that disrupt the balance of cytokines and chemokines, contributing to disease progression.[37,38] Microglia become reactive very early in life,[37] exhibiting both pro-inflammatory and anti-inflammatory actions. The specific mechanisms influencing their activation state during disease progression remain unclear.

In line with our findings, a recent study showed how the power of microglia transplantation in the CNS of Twi mice reduces psychosine content and extends the lifespan of these mice up to ~100 days,[39] which is coincident with the standard BMT therapy.

Given this context, we hypothesized that the uptake of GALC by microglia might influence cytokine profiles. Studies on mRNA expression levels of cytokines showed significant differences in IL-10, IFN-γ, and TREM2 at 10 days after EV-GALC treatment (Figures 5, 6 and 7). IL-10 is known for its ability to inhibit the production of pro-inflammatory cytokines by M1 microglia,[40,41] shifting towards an anti-inflammatory (M2) phenotype[42] and protecting neurons from excessive inflammation. In contrast, IFN-γ is associated with the activation of pro-inflammatory M1 classical, activated microglia, increasing the release of inflammatory cytokines such as TNF-α.[43] Our results showed a significant reduction in IFN-γ, supporting the idea that IL-10 may be effectively promoting the anti-inflammatory M2 phenotype, thereby mitigating

inflammation and potentially protecting neuroglial health.[44] It has been proposed that in KD, microglia exhibits a non-traditional "M3" phenotype, since shares features of both M1 and M2.[45] Hence, the differential regulation of the pro- and anti-inflammatory cytokines could also lead to a more complex regulation of the response of KD microglia. In this regard, our study also detected increased TREM-2. TREM-2 is critical for microglial activation and function, and its upregulation may reflect enhanced microglial activity.[46–49] This is particularly interesting, as it has been shown that the heterozygous mice for GALC ($GALC^{+/-}$) exhibit decreased expression of TREM-2, leading to impaired remyelination following cuprizone-induced demyelination.[50] Moreover, loss-of-function mutations in TREM-2 have been previously found to cause Nasu–Hakola leukodystrophy and are associated with increased risk in several neurodegenerative diseases.[51,52] Thus, TREM-2 is crucial for maintaining brain homeostasis by regulating microglial activity and facilitating repair processes. The uptake of GALC by microglia via EV-GALC ERT may have restored microglial function by upregulating TREM-2, thereby enhancing a positive regulation of neuroinflammation. Differential de novo synthesis of psychosine in each microglia sub-type has not been studied, and it could have contributed to lowering psychosine. Future experimentation will address psychosine synthesis in proinflammatory M1 vs anti-inflammatory M2 Twi microglial cells.

Elevated psychosine levels in the brain are associated with the emergence of cellular markers of inflammation and enhanced cytokine expression.[53] Although it is known that elevated levels of psychosine can be cytotoxic to myelinating cells, its direct role in immune activation is still emerging.[45,54] In this context, it is also plausible that cytokine-induced inflammation could indeed act as a parallel and overlapping mechanism alongside psychosine accumulation. A recent publication showed that depletion of GALC in microglia increases chemoattractant cytokines but does not affect psychosine levels.[55] This suggests that other inflammatory mediators or cellular stress responses trigger cytokine expression independently of psychosine levels. Investigating the detailed mechanisms through which cytokines and psychosine interplay can provide insights in the pathogenic mechanism of disease and lead to novel strategies to managing neuroinflammation and neurodegeneration in KD.

There is substantial potential for refining this therapeutic approach. We propose an ERT-EV-GALC paradigm that could: 1) utilize extracellular vesicles derived from mesenchymal stem cells (MSCs), and 2) engineer MSCs to produce GALC via adeno-associated virus or CRISPR-Cas technologies. MSCs have shown promise in reducing inflammation,[31] and we speculate that this property could enhance the efficacy of GALC delivery in the context of KD. Future research will be essential for developing a robust translational approach that could be applied not only to KD but also to other LSD and neurodegenerative diseases characterized by inflammation.

## Conclusion

This study demonstrates the potential of ERT mediated by EV-GALC as a novel transient strategy for addressing the metabolic and inflammatory hallmarks of KD in the Twi mouse model. Early delivery of GALC enzyme via EVs significantly reduced psychosine accumulation in the cortex, and alleviated neuroinflammation, particularly by shifting microglial activation towards an anti-inflammatory phenotype. The observed modulation of microglial activation, especially through TREM-2 and IL-10 upregulation, emphasizes the importance of targeting inflammation in managing KD and other lysosomal storage disorders (LSDs).

## Acknowledgments

This study was funded by the Rosenau Family Research Foundation (RFRF) to M.I.G and partially by UIC LASURI scholarship to D.G.

## Author Contributions

All authors made a significant contribution to the work reported, whether that is in the conception, study design, execution, acquisition of data, analysis and interpretation, or in all these areas; took part in drafting, revising or critically reviewing the article; gave final approval of the version to be published; have agreed on the journal to which the article has been submitted; and agree to be accountable for all aspects of the work.

## Disclosure

All authors declare that there is no competing interest in the preparation and execution of this work.

## References


1. Suzuki K. Twenty five years of the "psychosine hypothesis": a personal perspective of its history and present status. *Neurochem Res*. 1998;23(3):251–259. doi:10.1023/a:1022436928925
2. White AB, Givogri MI, Lopez-Rosas A, et al. Psychosine accumulates in membrane microdomains in the brain of Krabbe patients, disrupting the raft architecture. *J Neurosci*. 2009;29(19):6068–6077. doi:10.1523/JNEUROSCI.5597-08.2009
3. Igisu H, Suzuki K. Progressive accumulation of toxic metabolite in a genetic leukodystrophy. *Science*. 1984;224(4650):753–755. doi:10.1126/science.6719111
4. Kobayashi T, Goto I, Yamanaka T, Suzuki Y, Nakano T, Suzuki K. Infantile and fetal globoid cell leukodystrophy: analysis of galactosylceramide and galactosylsphingosine. *Ann Neurol*. 1988;24(4):517–522. doi:10.1002/ana.410240407
5. Biffi A. Hematopoietic stem cell gene therapy for storage disease: current and new indications. *Mol Ther*. 2017;25(5):1155–1162. doi:10.1016/j.ymthe.2017.03.025
6. Kwon JM, Matern D, Kurtzberg J, et al. Consensus guidelines for newborn screening, diagnosis and treatment of infantile Krabbe disease. *Orphanet J Rare Dis*. 2018;13(1):30. doi:10.1186/s13023-018-0766-x
7. Escolar ML, West T, Dallavecchia A, Poe MD, LaPoint K. Clinical management of Krabbe disease. *J Neurosci Res*. 2016;94(11):1118–1125. doi:10.1002/jnr.23891
8. Allewelt H, Taskindoust M, Troy J, et al. Long-term functional outcomes after hematopoietic stem cell transplant for early infantile Krabbe disease. *Biol Blood Marrow Transplant*. 2018;24(11):2233–2238. doi:10.1016/j.bbmt.2018.06.020
9. Rosenfeld MG, Kreibich G, Popov D, Kato K, Sabatini DD. Biosynthesis of lysosomal hydrolases: their synthesis in bound polysomes and the role of co- and post-translational processing in determining their subcellular distribution. *J Cell Biol*. 1982;93(1):135–143. doi:10.1083/jcb.93.1.135
10. Favret JM, Weinstock NI, Feltri ML, Shin D. Pre-clinical mouse models of neurodegenerative lysosomal storage diseases. *Front Mol Biosci*. 2020;7:57. doi:10.3389/fmolb.2020.00057
11. Muro S. Strategies for delivery of therapeutics into the central nervous system for treatment of lysosomal storage disorders. *Drug Deliv Transl Res*. 2012;2(3):169–186. doi:10.1007/s13346-012-0072-4
12. Lee WC, Courtenay A, Troendle FJ, et al. Enzyme replacement therapy results in substantial improvements in early clinical phenotype in a mouse model of globoid cell leukodystrophy. *FASEB J*. 2005;19(11):1549–1551. doi:10.1096/fj.05-3826fje
13. Weinstock NI, Shin D, Dhimal N, et al. Macrophages expressing GALC improve peripheral Krabbe disease by a mechanism independent of cross-correction. *Neuron*. 2020;107(1):65–81e9. doi:10.1016/j.neuron.2020.03.031
14. Dawson G. Quantum dots and potential therapy for krabbe's disease. *J Neurosci Res*. 2016;94(11):1293–1303. doi:10.1002/jnr.23805
15. Del Grosso A, Galliani M, Angella L, et al. Brain-targeted enzyme-loaded nanoparticles: a breach through the blood-brain barrier for enzyme replacement therapy in Krabbe disease. *Sci Adv*. 2019;5(11):eaax7462. doi:10.1126/sciadv.aax7462
16. Gigliobianco MR, Di Martino P, Deng S, Casadidio C, Censi R. New advanced strategies for the treatment of lysosomal diseases affecting the central nervous system. *Curr Pharm Des*. 2019;25(17):1933–1950. doi:10.2174/1381612825666190708213159
17. Thery C, Amigorena S, Raposo G, Clayton A. Isolation and characterization of exosomes from cell culture supernatants and biological fluids. *Curr Protoc Cell Biol*. 2006. doi:10.1002/0471143030.cb0322s30
18. Pergande MR, Kang C, George D, et al. Lipidomic analysis identifies age-disease-related changes and potential new biomarkers in brain-derived extracellular vesicles from metachromatic leukodystrophy mice. *Lipids Health Dis*. 2022;21(1):32. doi:10.1186/s12944-022-01644-8
19. Pituch KC, Moyano AL, Lopez-Rosas A, et al. Dysfunction of platelet-derived growth factor receptor alpha (PDGFRalpha) represses the production of oligodendrocytes from arylsulfatase A-deficient multipotential neural precursor cells. *J Biol Chem*. 2015;290(11):7040–7053. doi:10.1074/jbc.M115.636498
20. Sakai N, Inui K, Tatsumi N, et al. Molecular cloning and expression of cDNA for murine galactocerebrosidase and mutation analysis of the twitcher mouse, a model of Krabbe's disease. *J Neurochem*. 1996;66(3):1118–1124. doi:10.1046/j.1471-4159.1996.66031118.x
21. Marshall MS, Issa Y, Jakubauskas B, et al. Long-term improvement of neurological signs and metabolic dysfunction in a mouse model of krabbe's disease after global gene therapy. *Mol Ther*. 2018;26(3):874–889. doi:10.1016/j.ymthe.2018.01.009
22. Saldivia N, Heller G, Zelada D, et al. Deficiency of galactosyl-ceramidase in adult oligodendrocytes worsens disease severity during chronic experimental allergic encephalomyelitis. *Mol Ther*. 2024;32(9):3163–3176. doi:10.1016/j.ymthe.2024.06.035
23. Bedia C, Camacho L, Abad JL, Fabriàs G, Levade T. A simple fluorogenic method for determination of acid ceramidase activity and diagnosis of Farber disease. *J Lipid Res*. 2010;51(12):3542–3547. doi:10.1194/jlr.D010033
24. Lee WC, Tsoi YK, Troendle FJ, et al. Single-dose intracerebroventricular administration of galactocerebrosidase improves survival in a mouse model of globoid cell leukodystrophy. *FASEB J*. 2007;21(10):2520–2527. doi:10.1096/fj.06-6169com
25. Matthes F, Andersson C, Stein A, et al. Enzyme replacement therapy of a novel humanized mouse model of globoid cell leukodystrophy. *Exp Neurol*. 2015;271:36–45. doi:10.1016/j.expneurol.2015.04.020
26. Seras-Franzoso J, Díaz-Riascos ZV, Corchero JL, et al. Extracellular vesicles from recombinant cell factories improve the activity and efficacy of enzymes defective in lysosomal storage disorders. *J Extracell Vesicles*. 2021;10(5):e12058. doi:10.1002/jev2.12058
27. Flanagan M, Pathak I, Gan Q, et al. Umbilical mesenchymal stem cell-derived extracellular vesicles as enzyme delivery vehicle to treat morquio A fibroblasts. *Stem Cell Res Ther*. 2021;12(1):276. doi:10.1186/s13287-021-02355-0
28. Maqsood M, Kang M, Wu X, Chen J, Teng L, Qiu L. Adult mesenchymal stem cells and their exosomes: sources, characteristics, and application in regenerative medicine. *Life Sci*. 2020;256:118002. doi:10.1016/j.lfs.2020.118002
29. Wu H, Fu M, Liu J, et al. The role and application of small extracellular vesicles in gastric cancer. *Mol Cancer*. 2021;20(1):71. doi:10.1186/s12943-021-01365-z
30. Yuan Y, Sun J, You T, et al. Extracellular vesicle-based therapeutics in neurological disorders. *Pharmaceutics*. 2022;14(12). doi:10.3390/pharmaceutics14122652

31. Dabrowska S, Andrzejewska A, Lukomska B, Janowski M. Neuroinflammation as a target for treatment of stroke using mesenchymal stem cells and extracellular vesicles. *J Neuroinflammation*. 2019;16(1):178. doi:10.1186/s12974-019-1571-8
32. Abbasi-Kangevari M, Ghamari SH, Safaeinejad F, Bahrami S, Niknejad H. Potential therapeutic features of human amniotic mesenchymal stem cells in multiple sclerosis: immunomodulation, inflammation suppression, angiogenesis promotion, oxidative stress inhibition, neurogenesis induction, MMPs regulation, and remyelination stimulation. *Front Immunol*. 2019;10:238. doi:10.3389/fimmu.2019.00238
33. Campanella C, Caruso Bavisotto C, Logozzi M, et al. On the choice of the extracellular vesicles for therapeutic purposes. *Int J Mol Sci*. 2019;20(2). doi:10.3390/ijms20020236
34. Willis GR, Kourembanas S, Mitsialis SA. Therapeutic applications of extracellular vesicles: perspectives from newborn medicine. *Methods Mol Biol*. 2017;1660:409–432. doi:10.1007/978-1-4939-7253-1_34
35. Escolar ML, Poe MD, Provenzale JM, et al. Transplantation of umbilical-cord blood in babies with infantile Krabbe's disease. *N Engl J Med*. 2005;352(20):2069–2081. doi:10.1056/NEJMoa042604
36. Paolicelli RC, Bergamini G, Rajendran L. Cell-to-cell communication by extracellular vesicles: focus on Microglia. *Neuroscience*. 2019;405:148–157. doi:10.1016/j.neuroscience.2018.04.003
37. Snook ER, Fisher-Perkins JM, Sansing HA, et al. Innate immune activation in the pathogenesis of a murine model of globoid cell leukodystrophy. *Am J Pathol*. 2014;184(2):382–396. doi:10.1016/j.ajpath.2013.10.011
38. Potter GB, Petryniak MA. Neuroimmune mechanisms in krabbe's disease. *J Neurosci Res*. 2016;94(11):1341–1348. doi:10.1002/jnr.23804
39. Aisenberg WH, O'Brien CA, Sangster M, et al. Direct microglia replacement reveals pathologic and therapeutic contributions of brain macrophages to a monogenic neurological disease. *Immunity*. 2025;58(5):1254–1268e9. doi:10.1016/j.immuni.2025.03.019
40. Ledeboer A, Breve JJ, Wierinckx A, et al. Expression and regulation of interleukin-10 and interleukin-10 receptor in rat astroglial and microglial cells. *Eur J Neurosci*. 2002;16(7):1175–1185. doi:10.1046/j.1460-9568.2002.02200.x
41. Balasingam V, Yong VW. Attenuation of astroglial reactivity by interleukin-10. *J Neurosci*. 1996;16(9):2945–2955. doi:10.1523/JNEUROSCI.16-09-02945.1996
42. Laffer B, Bauer D, Wasmuth S, et al. Loss of IL-10 promotes differentiation of Microglia to a M1 phenotype. *Front Cell Neurosci*. 2019;13:430. doi:10.3389/fncel.2019.00430
43. Vila-del Sol V, Punzon C, Fresno M. IFN-gamma-induced TNF-alpha expression is regulated by interferon regulatory factors 1 and 8 in mouse macrophages. *J Immunol*. 2008;181(7):4461–4470. doi:10.4049/jimmunol.181.7.4461
44. Kwilasz AJ, Grace PM, Serbedzija P, Maier SF, Watkins LR. The therapeutic potential of interleukin-10 in neuroimmune diseases. *Neuropharmacology*. 2015;96(Pt A):55–69. doi:10.1016/j.neuropharm.2014.10.020
45. Nicaise AM, Bongarzone ER, Crocker SJ. A microglial hypothesis of globoid cell leukodystrophy pathology. *J Neurosci Res*. 2016;94(11):1049–1061. doi:10.1002/jnr.23773
46. Wang Y, Ulland TK, Ulrich JD, et al. TREM2-mediated early microglial response limits diffusion and toxicity of amyloid plaques. *J Exp Med*. 2016;213(5):667–675. doi:10.1084/jem.20151948
47. Deczkowska A, Keren-Shaul H, Weiner A, Colonna M, Schwartz M, Amit I. Disease-associated microglia: a universal immune sensor of neurodegeneration. *Cell*. 2018;173(5):1073–1081. doi:10.1016/j.cell.2018.05.003
48. Poliani PL, Wang Y, Fontana E, et al. TREM2 sustains microglial expansion during aging and response to demyelination. *J Clin Invest*. 2015;125(5):2161–2170. doi:10.1172/JCI77983
49. Cantoni C, Bollman B, Licastro D, et al. TREM2 regulates microglial cell activation in response to demyelination in vivo. *Acta Neuropathol*. 2015;129(3):429–447. doi:10.1007/s00401-015-1388-1
50. Scott-Hewitt NJ, Folts CJ, Hogestyn JM, Piester G, Mayer-Proschel M, Noble MD. Heterozygote galactocerebrosidase (GALC) mutants have reduced remyelination and impaired myelin debris clearance following demyelinating injury. *Hum Mol Genet*. 2017;26(15):2825–2837. doi:10.1093/hmg/ddx153
51. Guerreiro R, Wojtas A, Bras J, et al. TREM2 variants in alzheimer's disease. *N Engl J Med*. 2013;368(2):117–127. doi:10.1056/NEJMoa1211851
52. Rayaprolu S, Mullen B, Baker M, et al. TREM2 in neurodegeneration: evidence for association of the p.R47H variant with frontotemporal dementia and Parkinson's disease. *Mol Neurodegener*. 2013;8:19. doi:10.1186/1750-1326-8-19
53. Santambrogio S, Ricca A, Maderna C, et al. The galactocerebrosidase enzyme contributes to maintain a functional neurogenic niche during early post-natal CNS development. *Hum Mol Genet*. 2012;21(21):4732–4750. doi:10.1093/hmg/dds313
54. Ijichi K, Brown GD, Moore CS, et al. MMP-3 mediates psychosine-induced globoid cell formation: implications for leukodystrophy pathology. *Glia*. 2013;61(5):765–777. doi:10.1002/glia.22471
55. Favret J, Nawaz MH, Patel M, Khaledi H, Gelb M, Shin D. Perinatal loss of galactosylceramidase in both oligodendrocytes and microglia is crucial for the pathogenesis of Krabbe disease in mice. *Mol Ther*. 2024;32(7):2207–2222. doi:10.1016/j.ymthe.2024.05.019